# A Boussinesq Model for Breaking Waves: Comparisons with Experiments

Jayaram Veeramony[1] and Ib A. Svendsen[2]

**ABSTRACT:** *The paper describes results with a breaking wave model based on an extended set of Boussinesq equations. The wave breaking is described by accounting for the effect of vorticity generated by the breaking process. The vorticity field in the domain is obtained by solving the vorticity transport equation, which is based entirely on the Reynold's equations. In addition to the wave height decay and profile deformation predicted by earlier breaker models, the present model also provides information about the velocity profiles. The model results give good agreement with experimental data for wave height, setup and the velocity profiles. The cross-shore variation of the radiation stress calculated from the model results gives a good representation of the results from experimental data.*

## 1. Introduction.

Recently, there has been an increased need for time-domain modelling of breaking waves. This stems from a need to accurately model the nearshore wave motion and circulation. Simulations of breaking waves have been performed by Lin and Liu (1998a, 1998b). They solved the Reynolds equations for the mean flow and the $k - \epsilon$ equation for turbulent kinetic energy using the VOF method. The model results and experimental data were found to be in good agreement. The advantage of this type of modelling is that the flow details such as the turbulent intensities and the shear stresses can be directly evaluated from the model results. However, it takes about 48 hours of CPU time on a supercomputer to simulate one minute of real time for a two-dimensional case. As a

[1]Center for Applied Coastal Research, University of Delaware, Newark, DE. 19716 USA. email: jay@coastal.udel.edu

[2]Center for Applied Coastal Research, University of Delaware, Newark, DE. 19716 USA. email: ias@coastal.udel.edu

result, applications to practical cases are limited.

Hence, modelling of breaking waves using shallow water theories such as the nonlinear shallow water equations or the Boussinesq equations remain of practical importance. To incorporate breaking in such models, a wave breaking criterion and an energy dissipation mechanism is necessary. The wave breaking criteria used in all models are semi-empirical in nature, as there are no general theoretical bases on which a wave can be assumed to start breaking.

There are several ways in which the energy dissipation can be included in the models. One method is based on the concept of an artificial eddy viscosity term which is introduced in the momentum equations (see for example Zelt 1991; Karambas and Koutitas 1992; Wei and Kirby 1995). The value of the eddy viscosity is calibrated with experimental data. With suitable choices for the eddy viscosity, very good approximations to the wave height data is obtained. The problem with this approach is that the velocity profile is not changed from the standard quadratic profile (or a higher order polynomial depending upon the order of the terms retained in the Boussinesq theory) because the flow is modelled as a potential flow. The eddy viscosity term is also not physically justified.

Another method uses the concept of a roller model first used by Svendsen (1984a, 1984b). In these breaking models, the roller rides on the front face of the wave at the speed of the wave (Brocchini et al. 1991; Schäffer et al. 1992; Schäffer et al. 1993). This introduces a change in the velocity profile once the waves break. The velocity is assumed to have a constant value in the roller region equal to about 1.3 times the wave speed. Associated with this change in velocity profile is an excess momentum flux, which simulates wave breaking. As before, comparisons with experimental data show that the results for the wave heights and setup can be modeled quite accurately although the flow is essentially modelled as a potential flow. However, physically, the velocity profile assumed in such models is unrealistic.

Svendsen et al. (1996) presented a model for surf zone waves by accounting for the vorticity present in the breaking waves. The vertical distribution of the vorticity was obtained by solving the vorticity transport equation. The boundary condition was prescribed at the mean water level and a finite-difference scheme was used to solve the vorticity equation. However, though consistent with classical Boussinesq theory, this approach misses the significant contributions of the vorticity generated in the roller region. Also, by using a finite-difference scheme, it turns out that the small water depths in the surf zone resulted in significant numerical errors while resolving the vorticity distribution. The model used in

this paper is based on the same general principles. However, the boundary condition for vorticity is prescribed at the lower edge of the roller which is physically much more accurate. Furthermore, the vorticity equation is solved analytically, thus avoiding the problems associated with numerical modelling. Also, enhanced dispersion characteristics have been used.

## 2. Governing Equations.

The governing equations are derived from the basic equations for conservation of mass and momentum. The derivation, which is an extension of the classical Boussinesq theory with the Ursell number $U = O(1)$, was given in Svendsen et al. (1996). The Ursell number is defined as the ratio between the two parameters $\delta = a_0/h_0$ and $\mu = k_0 h_0$ where $a_0$, $h_0$ and $k_0$ are the characteristic wave amplitude, water depth and wave number respectively.

Then, the nondimensional depth integrated countinuity equation is

$$\frac{\partial \zeta}{\partial t} + \frac{\partial Q}{\partial x} = 0 \tag{1}$$

where $\zeta$ is the instantaneous water surface elevation and $Q$ is the volume flux.

The model uses the direct depth integrated version of the momentum equations, with the enhancement of the frequency dispersion suggested by Madsen et al. (1991), which is

$$\frac{\partial Q}{\partial t} + (h+\delta\zeta)\frac{\partial \zeta}{\partial x} + \delta\left(\frac{Q^2}{h+\delta\zeta}\right)_x - \mu^2\left(B+\frac{1}{3}\right)h^2(Q)_{xxt} - Bgh^3\zeta_{xxx} + \delta(\Delta M)_x + \mu^2(\Delta P)_{xxt} = 0 \tag{2}$$

where

$$\Delta M \equiv \int_{-h}^{\delta\zeta}(u_r^2 - \overline{u}_r{}^2)\,dz, \tag{3}$$

$$\Delta P \equiv \int_{-h}^{\delta\zeta}\frac{\partial^2}{\partial x \partial t}\int_z^{\delta\zeta}\frac{\partial}{\partial x}\int_{-h}^{z}(u_r - \overline{u}_r)\,dz\,dz\,dz \tag{4}$$

are the momentum signatures of breaking. In (3) and (4), the velocities are given by

$$u = \overline{u}_p + \mu^2\left(\frac{h}{2} - z\right)(h\overline{u}_p)_{xx} + \frac{\mu^2}{2}\left(\frac{h^2}{3} - z^2\right)\overline{u}_{p_{xx}} + u_r + O(\mu^4) \tag{5}$$

$$u_r \equiv \int_{-h}^{z}\omega\,dz - \mu^2\int_{-h}^{z}\int_{-h}^{z}\int_{-h}^{z}\omega_{xx}\,dz\,dz\,dz \tag{6}$$

where $\overline{u}_p$ is the depth-averaged velocity corresponding to the potential part of the flow (i.e. terms that do not include the vorticity) and $u_r$ is the rotational

part of the velocity which essentially represents the effect of breaking. $\omega$ is the vorticity.

Assuming a constant eddy viscosity, the vorticity transport equation and the boundary conditions read

$$\frac{\partial \omega}{\partial t} = \nu_t \frac{\partial^2 \omega}{\partial z^2} + O(\delta, \mu^2) \tag{7}$$

$$\omega(z = \zeta_e, t) = \omega_s(x, t) \tag{8}$$

$$\omega(z = -h, t) = 0 \tag{9}$$

$$\omega(z, t = 0) = 0 \tag{10}$$

where $\zeta_e$ is the lower edge of the roller and $\omega_s(x,t)$ is as yet unspecified. Noting that the terms involving breaking in (2) are $O(\delta)$ and $O(\mu^2)$, we keep only terms of $O(1)$ in the vorticity transport equation.

The bottom boundary condition of zero vorticity is consistent with the assumption that breaking is the most important source of vorticity. At the free surface we can expect zero vorticity along the part of the surface which does not include the roller region. In the roller region, measurements from hydraulic jumps (Svendsen et al. 1998) show that the free surface vorticity will also be close to zero. However, strong vorticity is generated inside the roller region with a maximum occuring near the lower limit of the roller. We approximate the vorticity generated in this region by the vorticity between the surface roller and the region beneath.

In the Svendsen et al. (1996) version of of the model, $\omega_s$ was specified along the mean water level rather than the lower limit of the roller. Though this is consistent with the Boussinesq assumptions, this turns out to be a major source of inaccuracy. Also, in the previous version of the model, the vorticity equations were solved using a Crank-Nicholson method. With the small water depths in the surf-zone, the numerical error due to the finite difference methods were also very large due to the necessity of a very fine discretization in $z$, unless a very fine discretization in $x$ and $t$ was also used. These deficiencies have been eliminated in the present version by introducing the coordinate transformation $\sigma = (h + z)/(h + \zeta_e)$ where $\zeta_e$ is $O(\delta)$. To $O(\delta, \mu^2)$ this gives (7) with $\sigma$ instead of $z$. Solving (7)-(10) analytically gives

$$\omega = \sigma \omega_s - 2 \sum_{n=1}^{\infty} G_n \sin n\pi\sigma, \tag{11}$$

where

$$G_n \equiv \frac{(-1)^{n+1}}{n\pi} \int_0^t \frac{\partial \omega_s}{\partial t} e^{n^2\pi^2\kappa(t-\tau)}\, d\tau. \tag{12}$$

Using (11), the expressions for $\Delta M$ and $\Delta P$ are obtained.

## 3. Boundary conditions for vorticity.

Measurements of velocity in the roller region for breaking waves are not yet available inside the surf-zone. However, velocity measurements are available for hydraulic jumps with for the range of Froude numbers $1 \simeq Fr < 2$ (Svendsen et al. 1998; Lin and Rockwell 1994; Bakunin 1995) which is similar to Froude numbers for breaking waves. Breaking waves viewed in a coordinate system which moves at the wave speed have flow patterns around the roller region that are very similar to that observed in hydraulic jumps. The absolute velocities and the bottom boundary layer would of course be different under this coordinate transformation but the turbulent stresses, the surface profile and especially the vorticity are the same in a moving coordinate system.

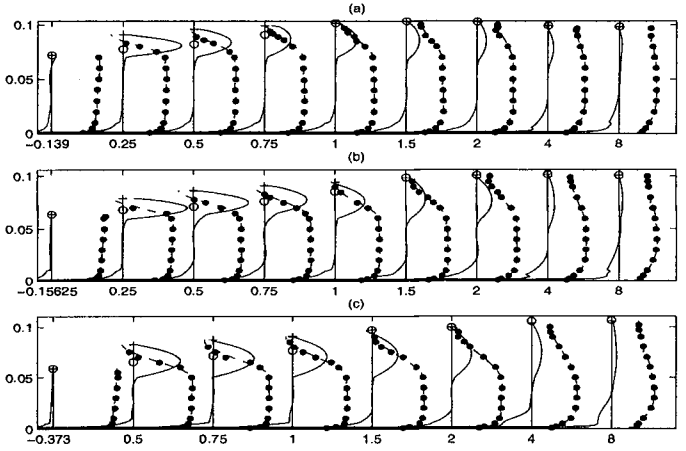


Figure 1: Velocity profiles in three hydraulic jumps with Froude numbers 1.38, 1.46 and 1.56. Data is '•', vorticity is '———' and the fit to the velocity is '– – –'. The total water depth at each location is '+' and the location of the lower edge of the streamline is 'o'(from Svendsen et al. 1998)

Velocity measurements by Bakunin (1995) were available for Froude numbers of 1.38, 1.46 and 1.56, from which the vorticity distribution could be calculated. The details of the analysis of the data can be found in Veeramony and Svendsen

(1997) and Svendsen et al. (1998). Figure 1 shows the variation of the horizontal velocity and the vorticity in the three jumps. The volume flux is also known for each jump condition from which the thickness of the roller is calculated, since the net volume flux through the roller region is zero. Figure 2a shows that the non-dimensional roller thickness is similar for all three cases. Therefore, the dimensionless roller thickness can be represented by the curve, obtained using a least squares fit to the data, shown in figure 2a.

$$\zeta_e = 0.78e^{x/l_r}\left(\frac{x}{l_r} - \frac{x^2}{l_r^2}\right) \tag{13}$$

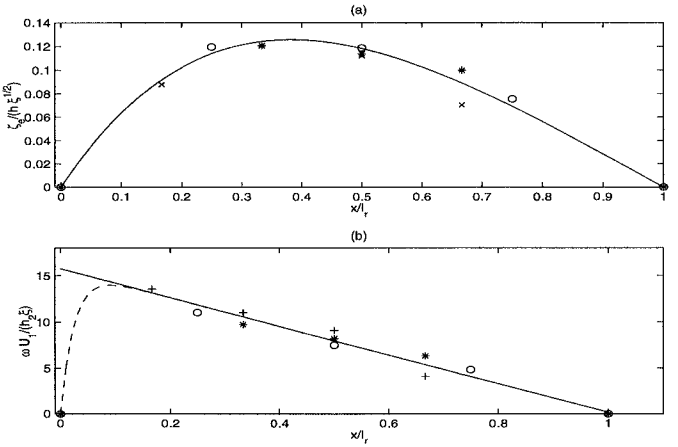


Figure 2: (a) The non-dimensional thickness of the roller for the hydraulic jumps: Data for Froude numbers 1.38 (o), 1.46 (x), 1.56(*) and least-squares fit (13). (b) Non-dimensional vorticity at the lower edge of the roller with the linear fit (———) and according to (14) (– – –).

Figure 2(b) shows the vorticity at the lower edge of the roller. Again, the non-dimensional values for all three cases are very similar, and the dimensionless $\omega_s$ can be represented by

$$\omega_s = 15.75\left(1 - \frac{x}{l_r}\right)$$

which is shown as the solid line in the figure. However, though physically realistic, the step discontinuity at $x/l_r = 0$ causes instabilities during the numerical evaluation of (12). To avoid this, we represent the vorticity by the expression

which is shown as the dashed line in figure 2b.

$$\omega_s = 15.75\left(1 - e^{40x/l_r}\right)\left(1 - \frac{x}{l_r}\right) \tag{14}$$

The expressions of $\zeta_e$ and $\omega_s$ from (13) and (14) are used in the solution (11) to the vorticity equation.

## 4 Comparison between model results and data.

The results from the model described in the previous section was compared to two sets of experiments with monochromatic waves. Wave heights and setup measurements for monochromatic waves are available from set of experiments by Hansen and Svendsen (1979). Wave shape and the velocity profiles below the wave trough are available from the measurements by Cox et al. (1995). Both experiments were conducted in wave flumes with plane beaches. The computational domain, shown in figure 3, is similar to the experimental domain. A

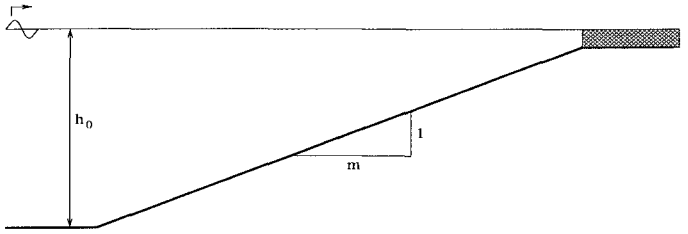


Figure 3: Schematic figure showing the computational domain. The shaded area represents the sponge layer and and the slope is $1{:}m$.

fourth-order ABM method is used to solve the equations numerically. Permanent form waves corresponding to (2) is used as input to the model. At the offshore boundary, an absorbing-generating boundary condition similar to that developed by Van Dongeren and Svendsen (1997) is used. A sponge layer is used to absorb the waves in the constant depth section which represents the shoreline. The wave is assumed to start breaking once the steepness at any point on the wave front is larger than 20°. Once the waves start breaking on a plane beach, it does not stop until it reaches the shoreline. The value of the eddy viscosity ($\nu_t$) used in the model is $0.05h\sqrt{gh}$ for all comparisons.

### *4.1 Wave height and set-up comparisons.*

The first set of comparisons is to the data from Hansen and Svendsen (1979). The experiments were conducted in a wave flume with a plain beach of slope 1:34.26. The water depth at the start of the slope was $h_0 = 0.36\ m$. Seven tests

| Case No. | $T$ $(secs)$ | $H$ $(cm)$ | $T\sqrt{g/h}$ |
|---|---|---|---|
| 1 | 3.3333 | 4.3 | 17.4 |
| 2 | 2.5 | 3.9 | 13.0 |
| 3 | 2.0 | 3.6 | 10.44 |

Table 1: Wave parameters from (Hansen and Svendsen 1979) at the toe of the beach.

were conducted in all. The wave heights and set-up for each case was measured at a number of locations. In this paper, comparisons will only be shown for three cases. Table 1 presents the wave period and the wave height at the start of the slope for each of the cases.

Figure 4 shows the comparison between the model results and the data for Case 1. The wave heights in the initial part of the shoaling region is represented well. As the waves get closer to breaking, the agreement between the model and data deteriorates. At the point of wave breaking, the difference between the two is very obvious. The reason for this discrepancy is that the present version of the potential part of the model is based on weakly nonlinear theory as in Madsen et al. (1997a, 1997b)

Though that can be improved, the emphasis of this study, however, is the modelling of the phenomena after breaking. A short while after the breaking has been initiated in the model, it is seen that the agreement is very good.

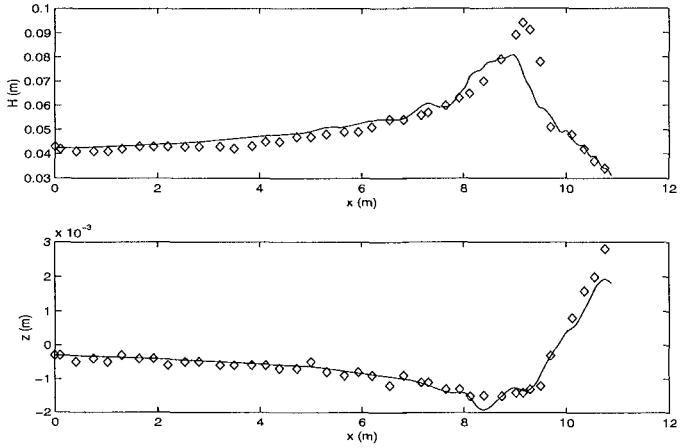


Figure 4: Comparison between model results (———) and data (o) from (Hansen and Svendsen 1979) of wave heights (a) and setup (b) for Case 1 in table 1.

An important gauge of the model performance is obtained from looking at the prediction of the set-up (figure 4b), which show good agreement between the model results and the experimental data. This suggests that the evaluation of such terms as the radiation stresses will also be accurate.

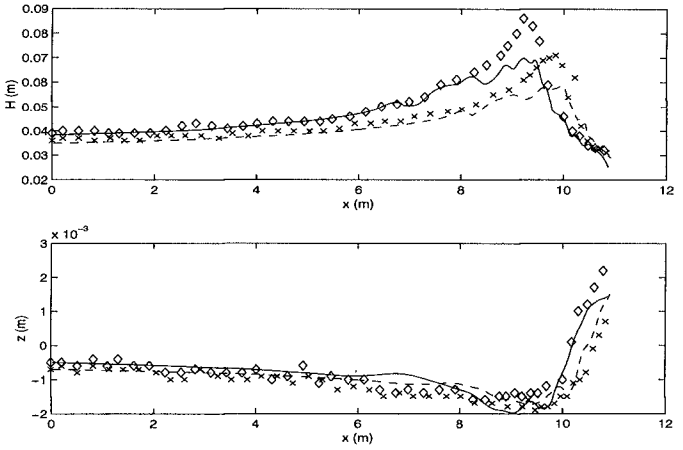


Figure 5: Comparison between model results and data from (Hansen and Svendsen 1979) of wave heights (a) and setup (b) for Case 2 (———is model, ◇ is data) and Case 3 (– – –is model, × is data) in table 1.

Figure 5 shows the comparisons for Cases 2 and 3. Again, the model underestimates the wave height near the breaking region. On the other hand, the prediction of the set-up is consistently good. All this indicates that the flow properties in the surf-zone are being modelled correctly. To illustrate this further, the results from the model are compared to velocity data from breaking waves in the next section.

## *4.2 Velocity and surface elevation comparisons to data.*

Velocity and surface elevation data were gathered by Cox et al. (1995). The experiments were conducted in a wave flume with a plain beach slope of 1:35. The wave height at the wavemaker was $H_0 = 11.5\ cm$ and the water depth at the start of the beach was $h_0 = 0.40\ m$. The wave period was $T_0 = 2.2\ secs$. Measurements of velocity in the vertical were taken at six locations given in table 2.

The first measuring line was outside the breaking region, the second was close to the breaking point and the last four were inside the surf zone. Comparisons

| Line No. | L1 | L2 | L3 | L4 | L5 | L6 |
|---|---|---|---|---|---|---|
| h (cm) | 28.0 | 21.14 | 17.71 | 14.29 | 10.86 | 7.43 |

Table 2: Location of measuring lines for the data of (Cox, Kobayashi, and Okayasu 1995)

will be shown again for three cases inside the surf-zone.

Figure 6 show the comparisons at the still water depths of $h = 17.71 cm$ (6a), $h = 14.29\ cm$ (6b) and $h = 10.86\ cm$ (6c). The $x$-axis in the figure is normalized by the wave period. The wave shape according to the model (– – –) does not have the saw-tooth shape seen in the data (———) at any location in the surf zone. To obtain a saw-tooth profile for the wave in the surf-zone it is necessary to have full non-linearity at least up to the order of dispersion that is retained. As a result, the weakly non-linear Boussinesq model will perform significantly worse in this regard than, say, the non-linear shallow water (NSW) model, although the NSW equations retain less terms than the Boussinesq equations. The comparison between the velocity profiles predicted by the model (–·–·–) and that obtained from measurements (o) are also shown in figure 6. For the most part, the agreement between the two are excellent. An exception is near the toe of the wave face ($t/T = 0.2$) where the model tends to predict a positive velocity whereas the data shows negative velocities. The differences are clearly due to the differences in the predicted and measured surface profiles.

Figure 7 shows the vorticity field in a breaking wave. The contour lines of vorticity (7a) show that the vorticity produced in the roller region is convected downward and towards the back of the wave. The maximum value of the vorticity in the wave is close to the toe of the roller as is expected. On the other hand, along each vertical cross-section, it is only in the initial region of the roller that the maximum of the vorticity is close to the lower edge of the roller. Behind approximately the halfway point between the start of the roller and the end, the maximum of the voriticty is below the lower limit of the roller. This result is similar to that observed in the hydraulic jumps (Figure 1). Thus, this important feature of the vorticity distribution is captured by the model, even though only terms upto $O(1)$ are retained in (7)-(10).

The results of the model for $u$ and $\zeta$ are used to compute the radiation stress. The radiation stress in the cross shore direction is defined as

$$S_{xx} = \overline{\int_{-h}^{\zeta} (\rho u^2 - p_D)\, dz} + \frac{1}{2}\rho\overline{(\zeta - \bar{\zeta})^2} \tag{15}$$

where the $\overline{()}$ denotes averaging over a wave period and $p_D$ is the dynamic pressure. To the lowest order of approximation that has been retained so far,

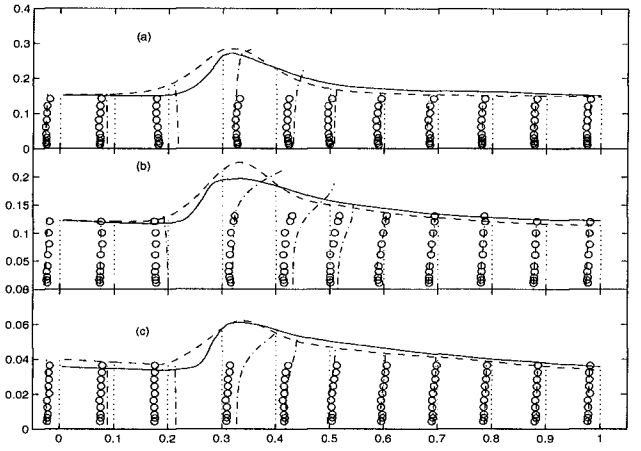


Figure 6: Comparison between model predictions and data from Cox et al. 1995 at $h = 17.71\,cm$ (a), $h = 14.29\,cm$ (b) and $h = 10.86\,cm$ (c) showing water surface elevations from model (– – –) and data (———) and velocity profiles from model (–·–·–) and data (o). The vertical lines (·····) show the locations at which the velocities are compared.

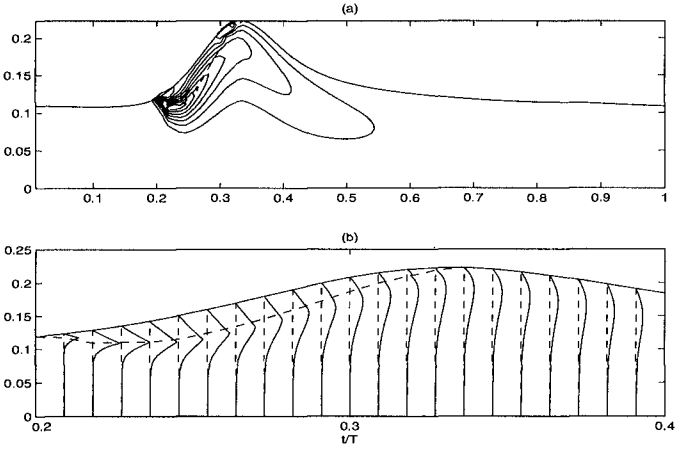


Figure 7: (a) Contours of vorticity at $L4$. (b) Vertical profiles of vorticity under the roller and behind the crest.

$p_D \simeq \rho w^2$ where $w$ is the vertical velocity.

Figure 8 shows the spatial variation of the dimensionless radiation stress defined as

$$P \equiv \frac{S_{xx}}{\rho g H^2}.$$

Linear theory predicts a constant value of $P = 0.1875$. Wave breaking in the model starts at $x \simeq 9.6\,m$. The value of $P$ at the start of breaking is relatively low due to the peaky shape of the waves (see Svendsen 1984b for a detailed discussion). Svendsen and Putrevu (1993) presented results from experimental data for the normalized radiation stress, which shows considerable variation from one data set to another. However, all results have the same feature that the value of $P$ starts at the breaker point with fairly low values, increases to a maximum and then decreases towards the shoreline. Although the results of the model do not show that $P$ quite reaches the value predicted by linear wave theory, the same trend is observed.

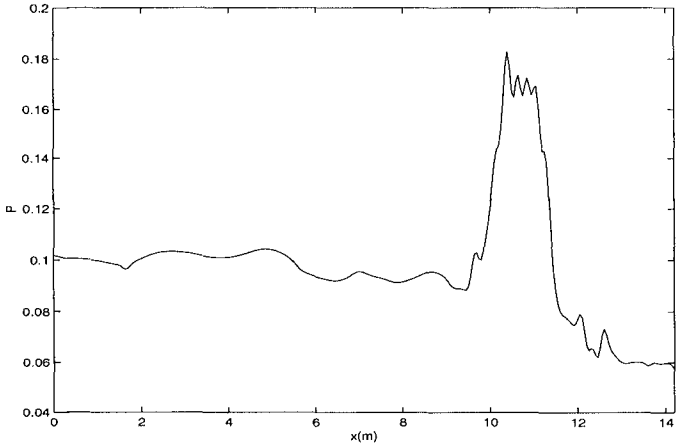


Figure 8: Spatial variation of the dimensionless radiation stress $P = S_{xx}/(\rho g H^2)$. Wave breaking starts at $x = 9.6\,m$. The sponge layer starts at $x = 15\,m$.

## 5 Conclusions.

The breaking model is an extension of the classical Boussinesq equations. The vorticity field in the domain is obtained by solving the lowest order vorticity transport equation, which is based entirely on the Reynold's equations. The boundary conditions for the solution for vorticity is parameterized using measurements from hydraulic jump. Comparisons with experimental data for

monochromatic waves show that the model performs well in the surf-zone. The wave heights are predicted reasonably accurately within the limitations of the form of the Boussinesq equations. The comparisons to the velocity profiles are especially good. The vorticity distribution calculated by the model agrees qualitatively with the results shown for hydraulic jump. The radiation stress in the cross-shore direction is calculated directly from the velocity field given by the model. The result is seen to agree qualitatively with that observed from other experiments.

## Acknowledgements.

This study was sponsored by the National Science Foundation under the grant OCE-9203277 and by the Office of Naval Research under contract No. 98PRO5167-00. The United States Government is authorized to produce and distribute reprints for government purposes notwithstanding any copyright notation that may appear herein.

# References

Bakunin, J. (1995). Experimental study of hydraulic jumps in low froude number range. Master's thesis, Center for Applied Coastal Research, University of Delaware, Newark, DE19711.

Brocchini, M., P. Cherubini, and L. Iovenitti (1991). An extension of boussinesq type model to the surf zone. *Computer Modelling in Ocean Engineering 91, Rotterdam, The Netherlands*, pp. 349–359.

Cox, D. T., N. Kobayashi, and A. Okayasu (1995). Experimental and numerical modeling of surf zone hydrodynamics. Technical Report CACR-95-07, Center for App. Coastal Res., University of Delaware.

Hansen, J. B. and I. A. Svendsen (1979). Regular waves in shoaling water: Experimental data. Technical report, ISVA Series Paper 21.

Karambas, T. K. and C. Koutitas (1992). A breaking wave propagation model based on the boussinesq equations. *Coastal Engineering 18*, pp. 1–19.

Lin, J. C. and D. Rockwell (1994). Instantaneous structure of a breaking wave. *Physics of Fluids 6(9)*, pp. 2877–2879.

Lin, P. and P. L. F. Liu (1998a). A numerical study of breaking waves in the surf zone. *Journal of Fluid Mechanics 359*, pp. 239–264.

Lin, P. and P. L. F. Liu (1998b). Turbulence transport, vorticity dynamics, and solute mixing under plunging breaking waves in surf zone. *Journal of*

*Geophysical Research 103*, pp. 15677–15694.

Madsen, P. A., R. Murray, and O. R. Sørensen (1991). A new form of boussinesq equations with improved dispersion characteristics. *Coastal Engineering 15*, pp. 371–388.

Madsen, P. A., O. R. Sørensen, and H. A. Schäffer (1997a). Surf zone dynamics simulated by a boussinesq type model. part i. model description and cross-shore motion of regular waves. *Coastal Engineering 32*, pp. 255–287.

Madsen, P. A., O. R. Sørensen, and H. A. Schäffer (1997b). Surf zone dynamics simulated by a boussinesq type model. part ii. surf beat and swash oscillations for wave groups and irregular waves. *Coastal Engineering 32*, pp. 289–319.

Schäffer, H. A., R. Deigaard, and P. A. Madsen (1992). A two-dimensional surf zone model based on the boussinesq equations. *Proceedings of the 23rd ICCE*, pp. 576–589.

Schäffer, H. A., P. A. Madsen, and R. Deigaard (1993). A boussinesq model for wave breaking in shallow water. *Coastal Engineering 20*, pp. 185–202.

Svendsen, I. A. (1984a). Mass flux and undertow in a surf-zone. *Coastal Engineering 8*, pp. 347–365.

Svendsen, I. A. (1984b). Wave heights and set-up in a surf-zone. *Coastal Engineering 8*, pp. 303–329.

Svendsen, I. A. and U. Putrevu (1993). Surfzone wave paramters from experimental data. *Coastal Engineering 19*, pp. 283–310.

Svendsen, I. A., J. Veeramony, J. Bakunin, and J. T. Kirby (1998). The flow in weak turbulent hydraulic jumps. *Submitted to the Journal of Fluid Mechanics*.

Svendsen, I. A., K. Yu, and J. Veeramony (1996). A boussinesq breaking wave model with vorticity. *Proceedings of the 25rd ICCE*, pp. 1192–1204.

Van Dongeren, A. R. and I. A. Svendsen (1997). Absorbing-generating boundary condition for shallow water models. *ASCE Journal of Waterway, Port, Coastal and Ocean Engineering 123*(6), pp. 303–313.

Veeramony, J. and I. A. Svendsen (1997). Analysis of the roller in hydraulic jumps. *To appear in the proceedings of Coastal Dynamics*.

Wei, G. and J. T. Kirby (1995). A coastal processes model based on time-domain boussinesq equations. *Coastal Dynamics*.

Zelt, J. A. (1991). The run-up of nonbreaking and breaking solitary waves. *Coastal Engineering 15*, pp. 205–246.